Electronic Supplementary Information

1. Experimental Section

1.1 Reagents and materials

Ammonium fluoride (AR), cobalt nitrate hexahydrate (AR), cupric nitrate (AR), urea (AR) and potassium hydroxide (AR) were provided by Aladdin Co., Ltd. Hydrochloric acid (AR), nitric acid (AR) and ethanol (AR) were purchased from Damao Chemical Corporation. RuO_2 and nafion (5 wt. %) were bought from Sigma-Aldrich Chemical Reagent Co., Ltd. All chemical regents were used as received without further purification. Prepare all standard solutions using deionized (DI) water with a resistance of 18.25 MΩ.

1.2 Preparation of Co(OH)F/NF and Cu doped Co(OH)F/NF

The Co(OH)F and Cu doped Co(OH)F on Ni foam (Cu-Co(OH)F/NF) were prepared by hydrothermal method. For Cu-Co(OH)F/NF, 50 ml deionized water containing 0.438 g cobalt nitrate hexahydrate, 0.05 g cupric nitrate, 0.135 g ammonium fluoride and 0.45 g urea added into a beaker with the mechanical stirring for 1 h. Then, the clear solution and Ni foam (4 cm × 2 cm) were transferred to a 100 ml teflon-lined autoclave. The autoclave was sealed and heat at 120 °C for 6 h in an electric oven. The resulting precursor was washed with deionized water for several times and and dried. Co(OH)F/NF was fabricated in the same method but without cupric nitrate.

1.3Preparation of Co_4N/NF,and Cu-Co_4N/NF

The obtained electrodes (CoOHF/NF and Cu-Co(OHF)/NF) were annealed in a box furnace at 450 °C in NH_3 for 2 h with a heating rate of 2 °C/min to convert into Co_4N/NF and Cu-Co_4N/NF.

1.4 Characterizations

X-ray diffraction (XRD) measurement was carried out on Bruker D8 Advanced diffractometer with

Cu Kα radiation under a constant voltage of 40 kV. The scanning electron microscopy (SEM) images were obtained on a Hitachi S-4800 scanning electron microscope at a voltage of 10 kV. Transmission electron microscopy (TEM) and high-resolution TEM (HRTEM) measurements were made on a Hitachi Jem-2100F transmission electron microscope. X-ray photoelectron spectroscopy (XPS) analysis was performed on a Kratos Axis Supra X-ray photoelectron spectrometer. The X-ray absorption spectroscopy (XAS) data was measured on BL44A1 of Shanghai Photon Source, NSRRC. The in situ Raman spectroscopy was conducted on a LabRAM HR Evolution spectrophotometer with 514 nm wavenumber of the excitation light source.

1.5 Electrochemical Measurements

The electrochemical experiments were carried out with a three-electrode system by using a CHI 760E electrochemical workstation, where the graphite plate (2*3 cm^2) and Ag/AgCl were used as the counter and reference electrodes, respectively. The Cu-Co_4N and Co_4N were used as the working electrodes. The potentials were converted to the reversible hydrogen electrode (RHE) according to the equation:

$$E\ (RHE) = E\ (Ag/AgCl) + (0.197 + 0.0591 \times pH)\ V$$

For peroxidation process, The catalyt were prepared using Cyclic voltammetry (CV) at 50 mV s^{-1} for 50 cycles. The linear sweep voltammetry (LSV) measurements were carried out at slow speed (2 mV s^{-1}) at room temperature (~25 °C). Electrochemical impedance spectroscopy (EIS) was recorded at Overpotential of 270 mV under frequency range from 1M Hz to 0.01 Hz with an amplitude of 10 mV. The equivalent circuit diagram is R_Ω in series with parallel modules C_{dl} and Rs. The C_{dl} element models the double-layer capacitance, R_Ω represents the uncompensated electrolyte resistance. The $R_{ct.}$ is related to the kinetics of the interfacial charge transfer reaction. The electrochemical active surface area (ECSA) was measured by C_{dl} method derived from CV measurements. The specific capacitance

we used 40 μF cm^{-2} for calculating ECSA. The CV were conducted from 0.14 to 0.24 V vs Ag/AgCl with scanning rates of 5 to 25 mV s^{-1}.

1.6 In-situ Raman spectra experiment

The Renishaw inVia Raman microscope was used for *In-situ* Raman experiments. The signals were collected using a water-immersion objective at the excitation laser source of 514 nm. The experiments were carried out with a three-electrode system in a homemade Raman cell. The Pt wire and Ag/AgCl were used as the counter and reference electrodes, respectively. The Co_4N and Cu-Co_4N were grown on carbon cloth as working electrodes to avoid the influence of Ni foam for experiments. *In-situ* Raman measurements were carried out using a CHI 760E electrochemical workstation at the applied potentials from OCP to 1.6 V *vs.* RHE in 0.1 M KOH.

1.7 Theoretical simulations

The calculation was performed in the framework of the density functional theory with the projector augmented plane-wave method, as implemented in the Vienna ab initio simulation package.[1] The projector augmented wave (PAW) potentials[2] with the Perdew-Burke Ernzerh of (PBE)[3] were performed to describe the nuclei-electron and the electron exchange correlation interactions. The cut-off energy for plane wave was set to 400 eV. The energy criterion for iterative solution of the Kohn-Sham equation was set to 10^{-5} eV. A vacuum layer of 15 Å was added perpendicular to the sheet to avoid artificial interaction between periodic images. The Brillouin zone integration was performed using a 3x3x1 k-mesh. Grimme's DFT-D3 methodology[4] was used to describe the dispersion interactions. In this system, the U correction for Co and Cu atoms was set as 8.5 eV and 4.0 eV, respectively.[5] All the structures are relaxed until the residual forces on the atoms have declined to less than 0.05 eV/Å. The reaction energies (ΔG) were obtained based on the below equation:

$$\Delta G = \Delta E_{DFT} + \Delta ZPE - T\Delta S$$

where ΔE_{DFT} is the reaction energy calculated from DFT; ΔZPE is the zero-point energy; ΔS is the change in entropy. The values of ΔZPE and ΔS were obtained by vibration frequency calculation.

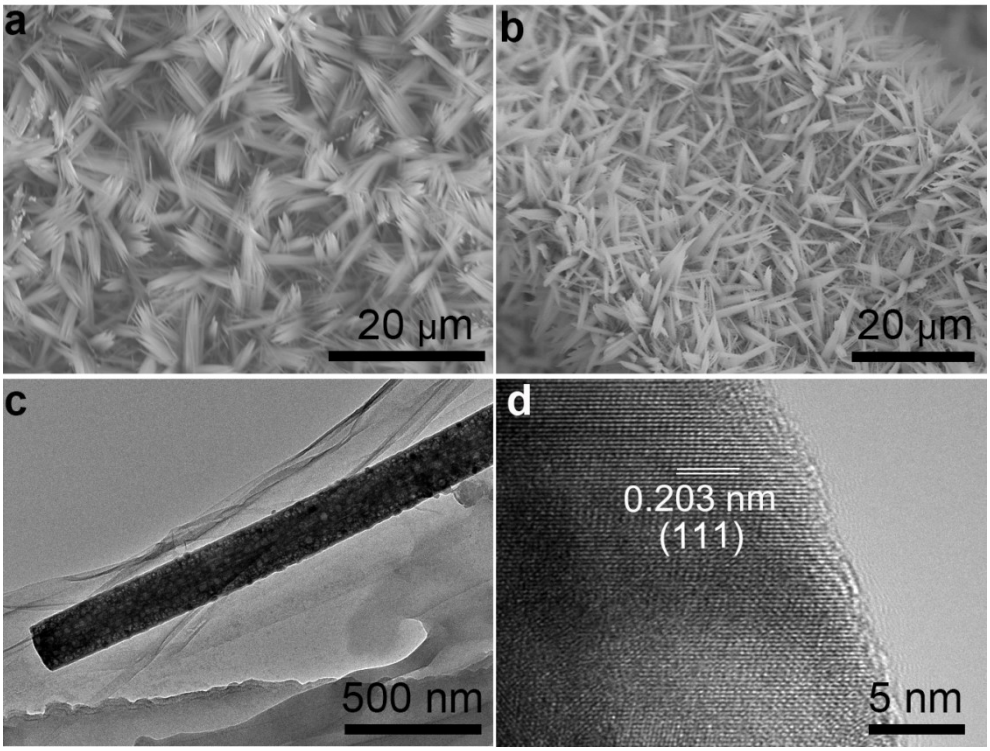

Fig. S1. The SEM images of (a) Co_4N and (b) Cu-Co_4N after OER. (c) TEM and (d) HRTEM images for Cu-Co_4N.

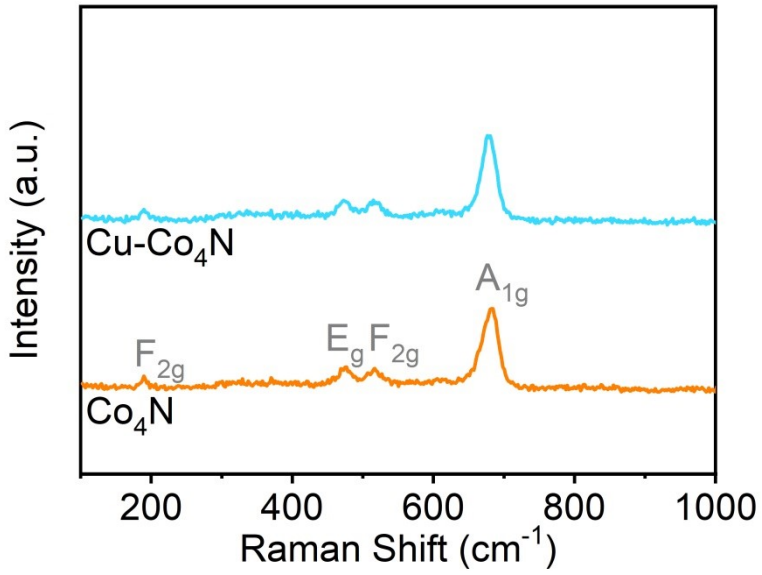

Fig. S2. Raman spectra of Co_4N and Cu-Co_4N.

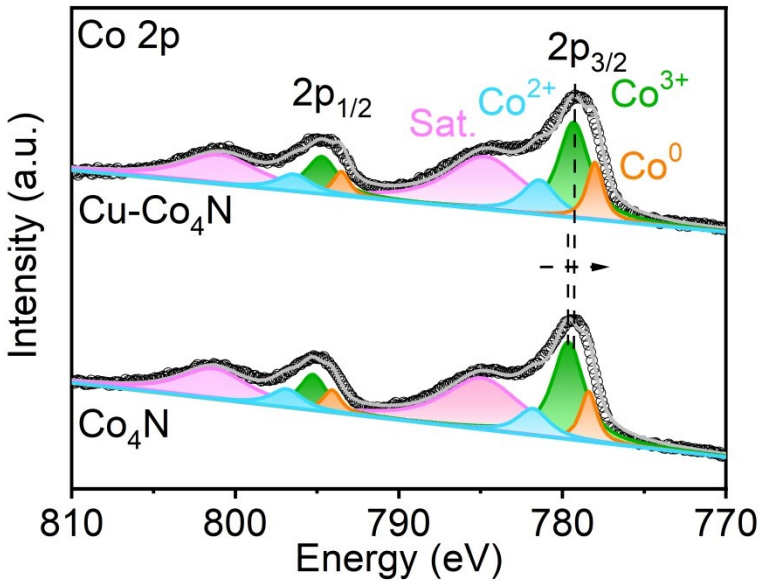

Fig. S3. XPS spectra in Co 2p regions for Cu-Co_4N and Cu-Co_4N after OER.

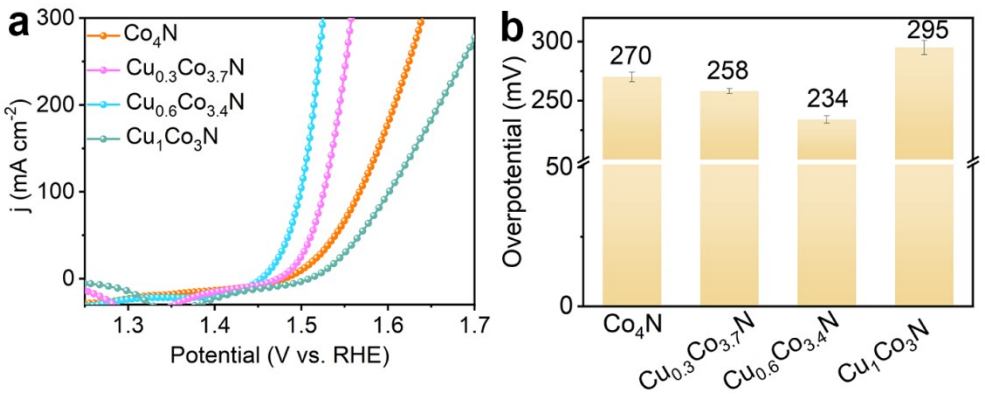

Fig. S4. (a) LSV curves of different ratios of Cu and Co, (b) the corresponding overpotentials at j = 10 mA cm^{-2}.

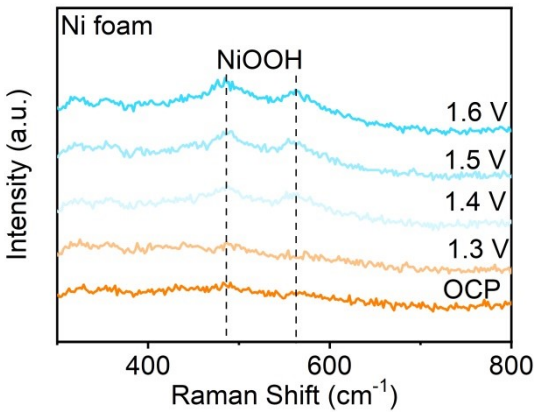

Fig. 5. *In-situ* Raman spectra of Ni foam at applied potentials from OCP to 1.6 V vs. RHE.

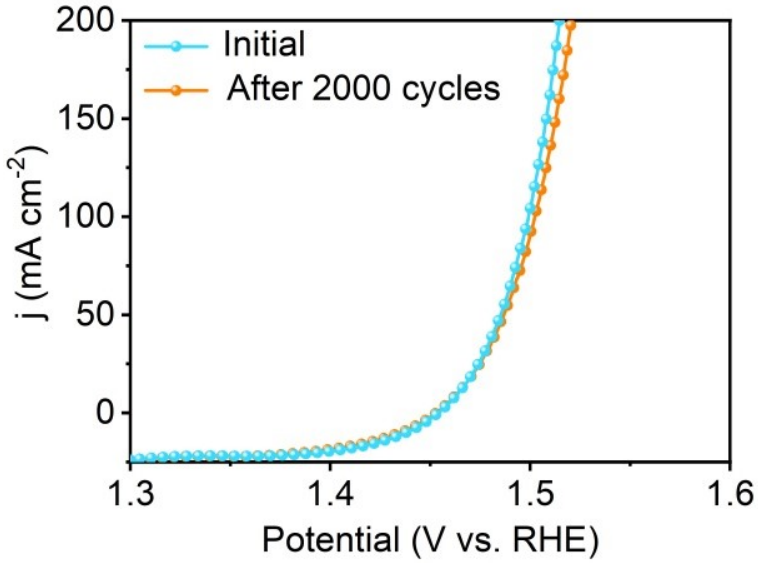

Figure S6. LSV curves of Cu-Co_4N before and after 2000 CV cycles.

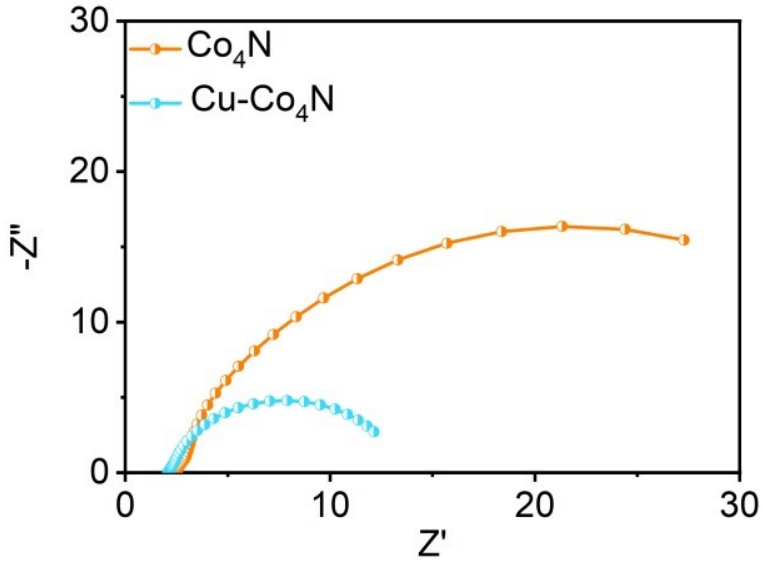

Figure S7. Nyquist plots of EIS for Cu-Co_4N and Co_4N.

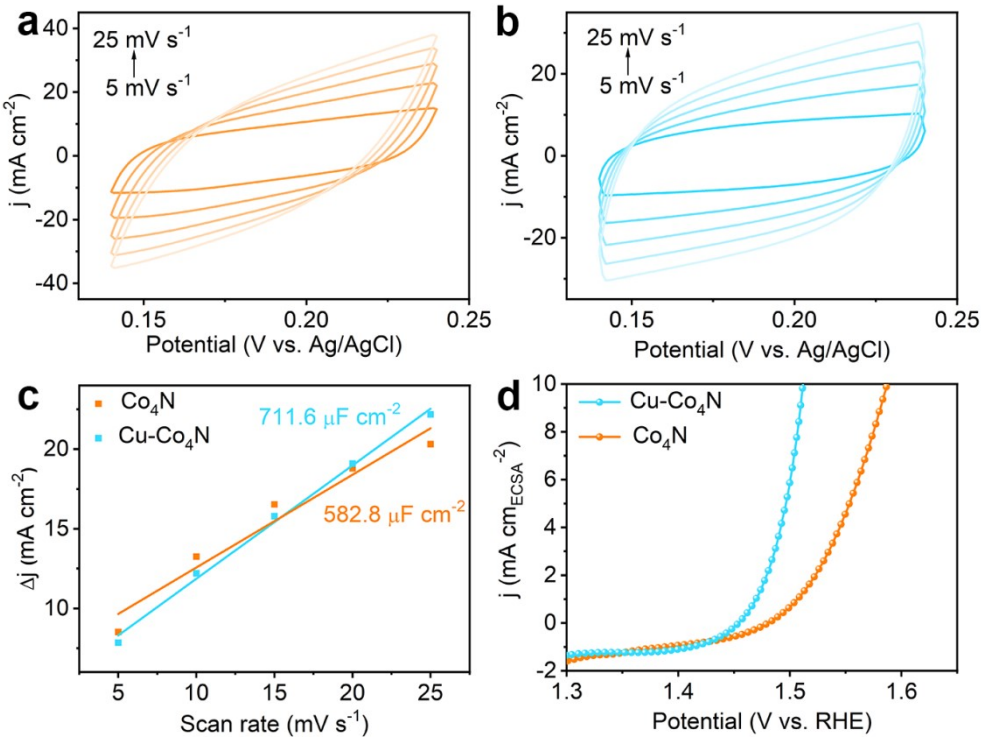

Fig. S8. CVs at various scan rates of 5, 10, 15, 20, and 25 mV s^{-1} for (a) Co_4N and (b) Cu-Co_4N. (c) The differences between capacitive currents at the center of selected potential window as a function of scan rate for Co_4N and Cu-Co_4N. (d) OER polarization curves normalized to the ECSA of Co_4N and Cu-Co_4N.

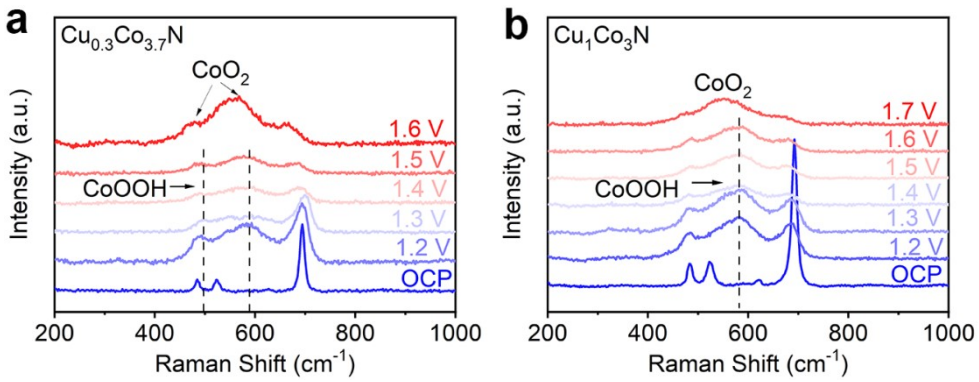

Fig. S9. *In-situ* Raman spectra of (a) Co_4N at applied potentials from OCP to 1.6 V *vs.* RHE and (b) Cu-Co_4N at applied potentials from OCP to 1.7 V *vs.* RHE.

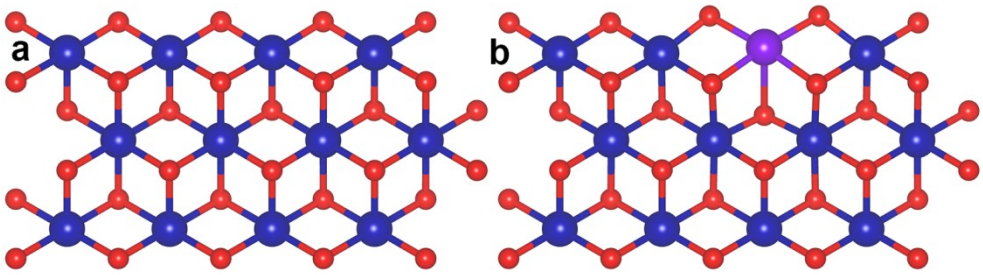

Fig. S10. Calculation models of (a) CoO_2 and (c) Cu-CoO_2. The blue, purple, red and white balls represent Co, Cu, O, and H atoms, respectively.

Table S1. Inductively coupled plasma mass spectrometry data for different ratios of Cu and Co.

	Cu Conc. [ppm]	Co Conc. [ppm]	Samples
1	15.9	202.2	$Cu_{0.3}Co_{3.7}N$
2	34.1	197.6	$Cu_{0.6}Co_{3.4}N$
3	48.2	141.13	Cu_1Co_3N

Table S2. Comparison of OER performance for Cu-Co_4N with other non-noble-metal electrocatalysts in alkaline media.

Catalysts	j (mA cm^{-2})	η (mV)	Tafel slope (mV dec^{-1})	Reference
Cu-Co_4N	**10** **50**	**234** **255**	**33.1**	**This work**
Gd-CoB	10	230	42	6
3DOM $Mg_xCo_{3-x}O_4$	10	370	76	7
Co-Mo-P/CoNWs	20	270	60	8
Fe-Co_3O_4	10	262	40	9
Co_2P/CoNPC	10	326	72.6	10
Co_3Mo/Cu	10	261	82	11
CoOOH-W_D-Co_V	50	298	46.2	12
CoOOH/Co_9S_8	10	240~246	86.4	13
V_L-CFZ	10	290	79	14
NiCo LDH-TPA	10	267	52.4	15
Triple layer Fe–Co–Ni MOF	10	254	51.3	16
$NiCo_{2-x}Fe_xO_4$ NBs	10	274	42	17
2D MOF-Fe/Co	10	238	52	18

Table S3. Inductively coupled plasma mass spectrometry data for electrolyte of Cu-Co_4N after 50 cycles CVs (surface reconstruction process) and 10/20 h chronoamperometric tests.

	Cu Conc. [ppm]	Co Conc. [ppm]	Samples
1	147.542	257.0	After 50 CVs (initial)
2	147.041	265.5	After 10 h chronoamperometric test
3	143.725	266.56	After 20 h chronoamperometric test

References

1. G. Kresse and D. J. P. R. B. C. M. Joubert, From ultrasoft pseudopotentials to the projector augmented-wave method, *Phys. Rev. B*, 1999, **59**, 1758-177.
2. P. Blochl, E. Blöchl and P. E. Blöchl, Projected augmented-wave method, *Phys. Rev. B,* 1994, **50**, 17953–17979.
3. J. P. Perdew, M. Ernzerhof and K. J. T. J. o. c. p. Burke, Rationale for mixing exact exchange with density functional approximations, *J. Chem. Phys.*, 1996, **105**, 9982-9985.
4. S. Grimme, J. Antony, S. Ehrlich and H. Krieg, A consistent and accurate ab initio parametrization of density functional dispersion correction (DFT-D) for the 94 elements H-Pu, *J. Chem. Phys.*, 2010, **132**, 154104.
5. Z.-F. Huang, J. Song, Y. Du, S. Xi, S. Dou, J. M. V. Nsanzimana, C. Wang, Z. J. Xu and X. Wang, Chemical and structural origin of lattice oxygen oxidation in Co–Zn oxyhydroxide oxygen evolution electrocatalysts *Nat. Energy*, 2019, **4**, 329-338.
6. T. ul Haq, S. A. Mansour, A. Munir and Y. Haik, Gold-supported gadolinium doped CoB amorphous sheet: a new benchmark electrocatalyst for water oxidation with high turnover frequency, *Adv. Funct. Mater.*, 2020, **30**, 1910309.
7. Y. Zhang, Z. Zhang, G. Jiang, A. H. Mamaghani, S. Sy, R. Gao, Y. Jiang, Y. Deng, Z. Bai, L. Yang, A. Yu and Z. Chen, Three-dimensionally ordered mesoporous Co3O4 decorated with Mg as bifunctional oxygen electrocatalysts for high-performance zinc-air batteries, *Nano Energy*, 2022, **100**, 107425.
8. V. H. Hoa, D. T. Tran, D. C. Nguyen, D. H. Kim, N. H. Kim and J. H. Lee, Molybdenum and phosphorous dual doping in cobalt monolayer interfacial assembled cobalt nanowires for efficient overall water splitting, *Adv. Funct. Mater.*, 2020, **30**, 2002533.
9. S. L. Zhang, B. Y. Guan, X. F. Lu, S. Xi, Y. Du and X. W. Lou, Metal Atom-doped Co_3O_4 hierarchical nanoplates for electrocatalytic oxygen evolution, *Adv. Mater.*, 2020, **32**, 2002235.
10. H. Liu, J. Guan, S. Yang, Y. Yu, R. Shao, Z. Zhang, M. Dou, F. Wang and Q. Xu, Metal–organic-framework-derived Co_2P nanoparticle/multi-doped porous carbon as a trifunctional electrocatalyst, *Adv. Mater.*, 2020, **32**, 2003649.
11. H. Shi, Y.-T. Zhou, R.-Q. Yao, W.-B. Wan, X. Ge, W. Zhang, Z. Wen, X.-Y. Lang, W.-T. Zheng and Q. Jiang, Spontaneously separated intermetallic Co_3Mo from nanoporous copper as versatile electrocatalysts for highly efficient water splitting, *Nat. Commun.*, 2020, **11**, 2940.
12. Y. Dou, D. Yuan, L. Yu, W. Zhang, L. Zhang, K. Fan, M. Al-Mamun, P. Liu, C.-T. He and H. Zhao, Interpolation between W dopant and Co vacancy in CoOOH for enhanced oxygen evolution catalysis, *Adv. Mater.*, 2022, **34**, 2104667.
13. N. Yao, G. Wang, H. Jia, J. Yin, H. Cong, S. Chen and W. Luo, Intermolecular energy gap-induced formation of high-valent cobalt species in CoOOH surface layer on cobalt sulfides for efficient water oxidation, *Angew.Chem. Int. Ed.*, 2022, **61**, e202117178.
14. Y. Jiang, Y.-P. Deng, R. Liang, N. Chen, G. King, A. Yu and Z. Chen, Linker-compensated metal–organic framework with electron delocalized metal sites for bifunctional oxygen electrocatalysis, *J. Am. Chem. Soc.*, 2022, **144**, 4783-4791.
15. W. Liu, D. Zheng, T. Deng, Q. Chen, C. Zhu, C. Pei, H. Li, F. Wu, W. Shi, S.-W. Yang, Y. Zhu and X. Cao, Boosting electrocatalytic activity of 3d-block metal (hydro)oxides by ligand-induced conversion, *Angew.Chem. Int. Ed.*, 2021, **60**, 10614-10619.
16. F. Shahbazi Farahani, M. S. Rahmanifar, A. Noori, M. F. El-Kady, N. Hassani, M. Neek-Amal, R. B. Kaner and M. F. Mousavi, Trilayer metal–organic frameworks as multifunctional electrocatalysts for energy conversion and storage applications, *J. Am. Chem. Soc.*, 2022, **144**, 3411-3428.
17. Y. Huang, S. L. Zhang, X. F. Lu, Z.-P. Wu, D. Luan and X. W. Lou, Trimetallic spinel $NiCo_{2-x}Fe_xO_4$ nanoboxes

for highly efficient electrocatalytic oxygen evolution, *Angew.Chem. Int. Ed.*, 2021, **60**, 11841-11846.

18. K. Ge, S. Sun, Y. Zhao, K. Yang, S. Wang, Z. Zhang, J. Cao, Y. Yang, Y. Zhang, M. Pan and L. Zhu, Facile synthesis of two-dimensional iron/cobalt metal–organic framework for efficient oxygen evolution electrocatalysis, *Angew.Chem. Int. Ed.*, 2021, **60**, 12097-12102.